



## Long-read RNA sequencing reveals allele-specific N6-methyladenosine modifications

Dayea Park and Can Cenik

*Genome Res.* published online October 29, 2024

Access the most recent version at doi:[10.1101/gr.279270.124](https://doi.org/10.1101/gr.279270.124)

---

<b>P&lt;P</b>	Published online October 29, 2024 in advance of the print journal.
<b>Accepted Manuscript</b>	Peer-reviewed and accepted for publication but not copyedited or typeset; accepted manuscript is likely to differ from the final, published version.
<b>Creative Commons License</b>	This article is distributed exclusively by Cold Spring Harbor Laboratory Press for the first six months after the full-issue publication date (see <a href="https://genome.cshlp.org/site/misc/terms.xhtml">https://genome.cshlp.org/site/misc/terms.xhtml</a> ). After six months, it is available under a Creative Commons License (Attribution-NonCommercial 4.0 International), as described at <a href="http://creativecommons.org/licenses/by-nc/4.0/">http://creativecommons.org/licenses/by-nc/4.0/</a> .
<b>Email Alerting Service</b>	Receive free email alerts when new articles cite this article - sign up in the box at the top right corner of the article or <a href="#">click here</a> .

---

---

Advance online articles have been peer reviewed and accepted for publication but have not yet appeared in the paper journal (edited, typeset versions may be posted when available prior to final publication). Advance online articles are citable and establish publication priority; they are indexed by PubMed from initial publication. Citations to Advance online articles must include the digital object identifier (DOIs) and date of initial publication.

---

To subscribe to *Genome Research* go to:  
<https://genome.cshlp.org/subscriptions>

---

Published by Cold Spring Harbor Laboratory Press

1 **TITLE**

2 Long-read RNA sequencing reveals allele-specific N<sup>6</sup>-methyladenosine modifications.

3

4 **RUNNING TITLE**

5 Allele-Specific N<sup>6</sup>-methyladenosine profiling

6

7 **AUTHORS**

8 Dayea Park<sup>1</sup>, Can Cenic<sup>1\*</sup>

9

10 **AFFILIATIONS**

11 <sup>1</sup> Department of Molecular Biosciences, University of Texas at Austin, Austin, TX 78712, USA

12

13 \* Corresponding author: [ccenic@austin.utexas.edu](mailto:ccenic@austin.utexas.edu)

14

15

16 **ABSTRACT**

17 Long-read sequencing technology enables highly accurate detection of allele-specific RNA

18 expression, providing insights into the effects of genetic variation on splicing and RNA abundance.

19 Furthermore, the ability to directly sequence RNA promises the detection of RNA modifications in

20 tandem with ascertaining the allelic origin of each molecule. Here, we leverage these advantages

21 to determine allele-biased patterns of N<sup>6</sup>-methyladenosine (m6A) modifications in native mRNA.

22 We utilized human and mouse cells with known genetic variants to assign allelic origin of each

23 mRNA molecule combined with a supervised machine learning model to detect read-level m6A

24 modification ratios. Our analyses revealed the importance of sequences adjacent to the DRACH-

25 motif in determining m6A deposition, in addition to allelic differences that directly alter the motif.

26 Moreover, we discovered allele-specific m6A modification (ASM) events with no genetic variants

27 in close proximity to the differentially modified nucleotide, demonstrating the unique advantage of  
28 using long reads and surpassing the capabilities of antibody-based short-read approaches. This  
29 technological advancement will advance our understanding of the role of genetics in determining  
30 mRNA modifications.

31

32 **Keywords:** LRS Special Issue, N<sup>6</sup>-Methyladenosine, Allele-specific expression

33

34

## 35 **INTRODUCTION**

36

37 Allele-specific expression (ASE) refers to the differences in gene expression from two alleles of  
38 the same gene. Such an imbalance in expression can contribute to phenotypic variation and the  
39 pathophysiology of diseases (Castel et al. 2015, 2020; Fan et al. 2020; de la Chapelle 2009;  
40 Gicquel et al. 2005). In mammalian development, a predominant form of ASE, genomic imprinting,  
41 plays a critical role as only one allele is expressed. Allele-specific DNA methylation and chromatin  
42 composition are two well-established epigenetic systems that control imprinted gene expression  
43 (Singh et al. 2010; Prendergast et al. 2012; Fournier et al. 2002).

44

45 ASE can reflect differential rates of transcription, mRNA stability, or alternative splicing between  
46 the alleles due to genetic variation (Amoah et al. 2021; Nembaware et al. 2008; Pai et al. 2012).  
47 That is, local genetic variants can influence transcriptional or post-transcriptional processes to  
48 modulate mRNA abundance of each allele (Robles-Espinoza et al. 2021). While the significance  
49 of allele-specific RNA expression is well-acknowledged, allele-specific RNA modification remains  
50 underexplored.

51

52 N<sup>6</sup>-Methyladenosine (m6A), the most prevalent RNA modification of mRNAs, has been suggested  
53 to impact diverse mechanisms to regulate gene expression (He and He 2021; Lee et al. 2020).  
54 Various interactions with the methyltransferase complex or m6A reader proteins impact several  
55 steps of mRNA metabolism, including splicing, export, translation, recruitment of RNA-binding  
56 proteins, and stability (Wang et al. 2022; Jiang et al. 2021; Lin and Gregory 2014; Akhtar et al.  
57 2021).

58  
59 Transcriptome-wide patterns of m6A RNA modifications have typically been studied using short-  
60 read sequencing coupled with either antibody-dependent methods such as MeRIP-seq (Meyer et  
61 al. 2012) or enzymatic/chemical approaches (Garcia-Campos et al. 2019; Meyer 2019a; Song et  
62 al. 2021). Among these methods, MeRIP-seq remains the most popular choice despite its  
63 limitations leading to elevated false-positive rates, attributable to nonspecific antibody binding  
64 (Helm et al. 2019; McIntyre et al. 2020; Zhang et al. 2021). Furthermore, all short-read sequencing  
65 strategies to detect m6A are inherently limited to aggregate measurements and are incapable of  
66 quantification at an individual molecular level.

67  
68 In contrast, Oxford Nanopore Technology (ONT) RNA sequencing enables direct detection of  
69 RNA modifications such as m6A with single molecule resolution (Garalde et al. 2018). The electric  
70 signal recorded by the ONT sequencing platform is altered by the presence of RNA modifications  
71 (Workman et al. 2018; Garalde et al. 2018; Pelizzola et al. 2021). Subsequently, machine learning  
72 methods can utilize the electronic current signal intensity to identify potential m6A sites from long-  
73 read data (Hendra et al. 2022).

74  
75 The ability to directly detect m6A modifications on the ONT RNA sequencing platform provides a  
76 unique opportunity to combine these advantages with the ability of long-read sequencing to  
77 facilitate ASE analysis. Long-read sequencing improves upon the fundamental limitations of short-

78 read sequencing for allele-specific analysis by detecting an increased number of single nucleotide  
79 polymorphisms (SNPs) on a read, enabling its precise allelic assignment (Cho et al. 2014). This  
80 feature has been leveraged to characterize the genetic effects of rare and common variants in  
81 the transcriptome (Glinos et al. 2022). Furthermore, long-read sequencing enables  
82 comprehensive analysis of splicing (Tilgner et al. 2015, 2018; Joglekar et al. 2021) which has  
83 fundamental importance for determining mRNA modifications due to their dependence on splicing  
84 patterns and transcript architecture (Yang et al. 2022; He et al. 2023; Cenik et al. 2017).

85

86 Here we introduce a novel approach harnessing ONT direct RNA sequencing (ONT DRS) to  
87 surmount the persistent constraints of m6A detection methods for allele-specific analyses. Our  
88 findings establish long-read sequencing of RNA as a robust solution for allele-specific m6A  
89 modification (ASM) analysis.

90

## 91 **RESULTS**

92

### 93 **ONT DRS enables the identification of allele-specific m6A modifications in hybrid mESCs**

94 We leveraged direct RNA sequencing (DRS) to simultaneously determine the allelic origin of each  
95 molecule along with its m6A modification status. To achieve high accuracy of allelic assignment  
96 of individual molecules, we used mouse embryonic stem cells (mESCs) that were derived from a  
97 cross of two highly genetically diverse mouse strains (C57BL/6J × CAST/EiJ, B6 × CAST)  
98 (Balasooriya and Spector 2022). Using DRS, we generated two replicates of 2.3 and 2.2 million  
99 reads from these hybrid mESCs.

100

101 To assess our ability to accurately detect m6A modifications, we generated mESC clones where  
102 methyltransferase-like 3 (*Mettl3*), the major methyltransferase for m6A modifications, is knocked  
103 out (Bokar et al. 1994; Liu et al. 2013) (Supplemental Fig. 1A, Supplemental Table 1; Methods).

104 As expected, in wild-type mESCs ~6% of the adenines within the context of a DRACH motif had  
105 a high-probability ( $>0.85$ ) of being modified, compared to only 0.2% in those with *Mettl3* knockout  
106 (Supplemental Fig. 1B). Among the sites displaying a high-probability modification ratio, the levels  
107 of modification ratios were consistently higher in wild-type compared to *Mettl3* knockout cells  
108 (Median modification ratio 0.629 and 0.512, respectively). Moreover, the modified adenines were  
109 predominantly clustered near the 3' end of coding sequences, which is consistent with the  
110 expected pattern of m6A RNA modifications (Meyer et al. 2012; Zhang et al. 2019) (Fig. 1A-B;  
111 Supplemental Fig. 1C-D).

112  
113 Using single nucleotide polymorphisms (SNPs), we assigned 1,110,260 (replicate 1) and 837,011  
114 (replicate 2) long-reads to their allelic origins across more than 13,000 transcripts (Fig. 1C,  
115 Methods). Of the detected transcripts, 8,657 transcripts had at least ten reads in both replicates.  
116 In allele-specific analyses, a common challenge is reference allele bias which is the tendency for  
117 reads that match the reference genome to align with a higher probability than reads containing  
118 the alternate allele, potentially skewing variant detection and analysis (Castel et al. 2015). To  
119 minimize this bias, we employed an N-masked transcriptome reference. This approach led to a  
120 mean CAST allele ratio across all transcripts of 0.505 as opposed to 0.485 when using an  
121 unmasked reference (Methods). These assignments were based on 135,380 (replicate 1) and  
122 134,585 (replicate 2) informative positions on the long-reads that overlapped known genetic  
123 variation between the strains (210,004 total SNPs).

124  
125 As an orthogonal approach to determine ASE, we used Illumina short-read sequencing. We found  
126 that RNA expression levels from the two methods were significantly correlated (Supplemental Fig.  
127 2A; Spearman's Correlations ( $\rho$ ), 0.792-0.816 across replicates). Moreover, gene-level allele-  
128 specific RNA expression was moderately concordant between the two approaches (Supplemental  
129 Fig. 2B; weighted  $\rho = 0.61$ , Methods). Although short-read sequencing produced nearly eight

130 times more aligned reads, long-read sequencing identified 2.3 times as many SNPs,  
131 demonstrating that the greater number of informative positions in long-read data enhances allelic  
132 assignment accuracy and gene-specific ASE reproducibility ( $\rho = 0.63$  and  $0.51$  for long-read  
133 and short-read sequencing, respectively; Supplemental Fig. 2C-D). Taken together, these  
134 measures of quality control underscore the high precision in allelic assignment.

135

136 We then employed a supervised machine learning approach (Hendra et al. 2022; Liu et al. 2019)  
137 to quantify m6A RNA modifications for the reads attributed to each allele. This process revealed  
138 an equivalence in the number of reads and m6A sites among alleles, indicating the allelic  
139 impartiality of our approach. Specifically, we observed similar numbers of reads (564,944 and  
140 444,514 for B6; 557,787 and 443,131 for CAST) and potential modification sites (114,457 and  
141 105,190 for B6; 112,947 and 105,117 for CAST) for each allele (Fig 2A, Supplemental Table 2).  
142 This result indicates minimal to no allelic bias in the assignment of reads and identification of  
143 modification sites.

144

145 The modification ratios of the candidate m6A sites were highly correlated between replicates and  
146 demonstrated an even higher correlation within the same allele. Specifically,  $\rho$  within the same  
147 allele were 0.82 and 0.83 for the modification ratios of the B6 and CAST allele, respectively.  
148 Conversely, correlations between different alleles were slightly lower, with the values of 0.77 (B6  
149 replicate 1, CAST replicate 2) and 0.75 (CAST replicate 1 and B6 replicate 2). In contrast,  
150 modification ratios from *Mettl3* knockout cells exhibited significantly lower correlations, falling  
151 below 0.46 (Fig. 2B, Supplemental Fig. 3).

152

153 To identify allele-specific m6A modifications, we established a selection criterion centered on a  
154 site probability aggregated from all reads. Therefore, we focused on m6A sites that demonstrated  
155 a high probability of modification ( $>0.85$ ) across reads. In mESC wild-type, an average of ~7% of

156 these candidate sites met our selection criteria. Notably, these m6A modification sites were  
157 predominantly localized at the junction between the coding region and the 3' UTR, showing high  
158 modification ratios (with median ratios of 0.621 for B6 and 0.627 for CAST; Fig. 2A, C,  
159 Supplemental Table 3). In contrast, *Mettl3* knockout had only 0.8% allelic sites exhibiting high  
160 probabilities of m6A modification. Moreover, these sites demonstrated a wider dispersion across  
161 various transcript regions (Fig. 2A, D). Overall, these observations affirm the ability of our  
162 methodology in detecting allelic m6A modifications subsequent to the assignment of reads to  
163 alleles.

164

### 165 **Detection of sites with significant allele-specific m6A modification**

166 The capability to accurately assign each RNA molecule to its allelic origin while concurrently  
167 identifying RNA modifications allows for the investigation of positions within mRNAs that exhibit  
168 differential modifications between alleles. While numerous statistical methods have been  
169 developed to identify allele-specific differences in gene expression phenotypes (DeVeale et al.  
170 2012), these studies underscore the challenges inherent in this analysis, including a propensity  
171 for false positives when employing simple binomial tests to assess deviations from expected  
172 expression levels across the two alleles (Zitovsky and Love 2019; Mohammadi et al. 2017).

173

174 To address these challenges, we implemented a conservative strategy that leverages bootstrap  
175 sampling to quantify uncertainty in modification ratio estimates (Methods). This method enabled  
176 us to pinpoint mRNA positions showing significant allele-specific m6A modification (ASM) (Fig.  
177 3A). Among detected 14,609 and 13,542 candidate m6A sites in the replicate experiments, we  
178 identified 57 ASM sites (FDR<0.1) with an average modification difference between the two alleles  
179 of 0.32.

180

181 In allele-specific analysis, previous research revealed that events with larger effect sizes are more  
182 likely to be reproducible and biologically relevant (Castel et al. 2020; Mohammadi et al. 2017).  
183 Therefore, we repeated our statistical analyses using an effect size threshold of 0.1 corresponding  
184 to the inferred modification ratio difference between the two alleles (Methods). This analysis  
185 uncovered 23 sites across 22 genes indicating ASM. Notably, at these ASM sites, the distributions  
186 of the resampled modification ratios from the two alleles were consistently distinct and had large  
187 effect sizes, with a mean modification ratio difference of 0.48 (Fig. 3B, Supplemental Fig. 5A,  
188 Supplemental Table 4). We focused our detailed analyses on this subset of ASM sites.

189  
190 One inherent limitation of ONT sequencing lies in its limited sequencing depth. Consistently,  
191 transcripts with statistically significant ASM sites had significantly greater RNA expression levels  
192 than those without, underscoring the dependence of ASM detection on transcript abundance  
193 (Supplemental Fig. 4).

194  
195 The genes with ASM sites are distributed across chromosomes without any discernible location  
196 preferences (Supplemental Fig. 5B), and are associated with a wide range of functions (Fig. 3C).  
197 A particularly notable finding was the identification of two distinct sites of ASM on the *Armc10*  
198 transcript, which encodes a protein involved in mitochondrial dynamics (Chen et al. 2019; Serrat  
199 et al. 2014). Moreover, our analysis identified six B6-biased ASM sites with a higher modification  
200 ratio on the B6 allele and 17 CAST-biased ASM sites with a higher ratio on the CAST allele. While  
201 the majority of ASM sites were located on 3' UTRs, one B6-biased ASM (on *Dnpep*) and two  
202 CAST-biased ASMs (on *Gnpat*, and *Pml*) were found in coding regions, near the stop codons  
203 (Supplemental Fig. 5C).

204  
205 Genome sequencing was used to identify genetic differences between the mouse inbred lines  
206 (Tsang et al. 2005; David J. Adams, Anthony G. Doran, Jingtao Lilue & Thomas M. Keane 2015),

207 however, potential genotyping errors from these could result in erroneous ASM calls. Hence, we  
208 verified the genomic DNA sequences near the m6A modification sites using Sanger sequencing  
209 (Supplemental Table 5, Methods). In six selected ASM sites, we confirmed annotated SNPs  
210 (*Nudt1*, D site), and the absence of unannotated genetic variants. These results indicate that the  
211 detected modifications are genuinely post-transcriptional and do not reflect genotyping errors.  
212 Taken together, these findings highlight a key strength of our approach based on the ONT DRS  
213 technique, which enables the detection of m6A modifications at the individual molecule level,  
214 rather than relying on aggregate measurements.

215

### 216 **Genetic variants influence allele-specific m6A modification patterns**

217 We hypothesized that local genetic differences could influence methylation efficacy, leading to  
218 differential m6A deposition. Accordingly, we categorized ASM-biased sites into two groups based  
219 on the proximity of the nearest genetic variation to the canonical m6A methylation motif (DRACH)  
220 (Fig. 3D-E). Of the 23 sites identified, six had genetic variants located within the DRACH motif  
221 itself (Group 1), with three variants at the D position, one at R, and two at H (Fig. 4A). In total, 41  
222 m6A sites had SNPs in D, R, or H positions, with 6 of these (14%) classified as ASM. These  
223 results suggest that SNPs within the DRACH motif are, as expected, more likely to lead to ASM.  
224 Furthermore, specific instances of the DRACH motifs are more likely to lead to modified adenines  
225 (Fig. 4B). In agreement with expectation, alleles for Group 1 ASM sites that exhibited higher  
226 modification ratios were more likely to match instances of the DRACH motif with higher propensity  
227 for modification (sole exception site on *Pml*).

228

229 Analysis of the remaining 17 sites (Group 2) revealed that five possessed genetic differences  
230 adjacent to the DRACH motif. Specifically, we found six SNPs near five m6A sites: *L3mbtl2* (D-1  
231 and H+1); *Trim25* and *Dnpep* (D-1); *Atmin* and *Tmbim6* (H+2) (Fig. 4C). Notably, all instances of  
232 SNPs at the D-1 position included a U at the D-2 position (UNUGACU). In this context, a cytosine

233 at the D-1 site correlated with higher m6A levels (*Dnpep*, 0.768; *Trim25*, 0.855; *L3mbtl2*, 0.789)  
234 compared to an adenine or a guanine at the D-1 site (adenine on *Dnpep*, 0.324 and *Trim25*, 0.073;  
235 guanine on *L3mbtl2*, 0.157; Fig. 4D). This finding highlights the significant influence of nucleotides  
236 adjacent to the DRACH motif on m6A deposition, contingent upon their specific genetic context.

237

238 Among remaining Group 2 ASM sites, eight had a SNP within 100 base pairs of the modified  
239 adenine (*Stk38*, -64; *2810004N23Rik*, -51; *Cmtm7*, -12 bp; *Glimp*, +10 bp; *Rsl1d1*, +34 bp; *Gcsh*,  
240 +42 bp; *Kif11*, +59; *Armc10* at 1170 position, +99). Despite the limitations imposed by the read  
241 length, short-read based m6A detection methods are theoretically capable of detecting SNPs  
242 within 50 to 100 bp of the methylated site (Dominissini et al. 2012; Chen et al. 2015). However,  
243 our method also identified four ASM sites that had no SNPs within this range hence highlighting  
244 the unique strength of long-read sequencing for ASM detection.

245

246 We also noticed that Group 2 ASMs were highly enriched for the UGACU motif sequence over  
247 the most commonly observed GAACU instance of the DRACH among m6A modified sites (Fig.  
248 4E, p-value of 0.0084, Methods). This finding suggests that ASM may be more prevalent for  
249 specific motif sequences distinct from those typically seen in m6A modified sites. In summary, we  
250 uncovered differential m6A modification of alleles that may depend on genetic differences that  
251 are proximal to the DRACH motif as well as ASM sites which have no nearby genetic differences.

252

### 253 **Validation of ASM sites through orthogonal approaches**

254 We next assessed the robustness of ASM detection by visualizing read pileups and conducting  
255 an orthogonal experimental method. Computational approaches to detect m6A modifications from  
256 direct RNA sequencing have been developed to leverage the increased propensity of base-calling  
257 errors around modified bases (Liu et al. 2019). We visualized sequencing reads that overlap ASM  
258 sites, enabling us to verify the expected enrichment of base-calling errors around sites with a

259 higher modification ratio. The phenomenon was observed consistently across both replicates,  
260 characterized by a correspondence between base-calling errors and modification ratios  
261 (Supplemental Fig. 6).

262

263 An orthogonal experimental approach that can potentially detect transcript regions with ASM is  
264 MeRIP-seq (Cao et al. 2023). MeRIP-seq relies on antibodies to differentiate modified loci and  
265 utilizes short-read sequencing; thus, this strategy lacks single-molecule and single-nucleotide  
266 resolution. Nonetheless, we reasoned that some ASM sites would overlap MeRIP-seq peaks and  
267 provide additional experimental support for allelic bias.

268

269 Among the 23 ASM sites, we detected 19 in the MeRIP-seq. Only four out of 19 sites, which  
270 contain SNPs within or nearby the DRACH motif had sufficient coverage in our MeRIP-seq data  
271 (Supplemental Table 6, Method). The allele bias ratio measured from MeRIP-seq in these four  
272 sites demonstrated consistency with the allele bias detected by our approach (Supplemental Fig.  
273 7). For example, *Atp5po* (Group 1 ASM) displayed allelic bias consistent with expectation in all  
274 three MeRIP-seq replicates (Fig. 4F). Another Group 2 ASM site, *Gcsh* (SNP at position 1,253,  
275 42 bp downstream of methylation site), exhibited the same allele-bias pattern in both long-read  
276 sequencing and MeRIP-seq data (Fig. 4G). In short, while MeRIP-seq cannot capture all ASM  
277 sites detected by the long-read approach due to inherent limitations, we observed consistent allele  
278 bias in m6A patterns at four sites with sufficient read coverage.

279

280 The reliance of MeRIP-seq on short-read sequencing can lead to errors in allelic assignment,  
281 primarily due to dependence on a limited number of SNPs, which increases susceptibility to  
282 reference allele bias, genotyping errors, and systematic biases in library preparation. To assess  
283 potential genotyping errors, we examined 37 SNP sites within ASM genes using Sanger  
284 sequencing. Of these, 33 sites showed the expected genetic variants with strong peak signals,

285 however, four sites (*Atp5po*, 776; *Psrc1*, 977; *Trim25*, 5007, and 5041) displayed nucleotides  
286 from only one allele suggesting potential genotyping errors or limitations in our Sanger  
287 sequencing experiments. Importantly, these findings further underscore the challenges of  
288 accurate allelic detection especially for the short-read sequencing approach that rely on a one or  
289 few SNPs (Supplemental Table 7).

290

### 291 **Applicability of ONT DRS to detect ASM sites in human cells**

292 The analytical and empirical workflow we developed to detect ASM sites is broadly applicable to  
293 any cell type with known genetic information. Given that systematic replication is essential to  
294 validate new approaches (Piccolo and Frampton 2016), we next replicated ASM detection using  
295 a lymphoblastoid cell line derived from a human with a well characterized genome. Specifically,  
296 we analyzed five replicates of ONT DRS data generated using the NA12878 cell line (Hansen  
297 2016; Workman et al. 2018), assigned reads to their allelic origin, and quantified m6A  
298 modifications for each group of reads (Fig. 5A, Supplemental Table 8).

299

300 Unlike hybrid mESCs, a typical human harbors many fewer heterozygous SNPs per transcript  
301 (Rozowsky et al. 2011; Workman et al. 2018). In our long-read sequencing analysis, among  
302 21,569 mouse transcripts, 16,242 contain at least one heterozygous SNP in hybrid mESCs, while  
303 only 8,889 human transcripts contain such sites in NA12878. The transcriptome overall harbors  
304 nearly ten times fewer heterozygous SNPs in NA12878 compared to hybrid mESCs (210,004 in  
305 mESCs; 27,269 in NA12878; Supplemental Fig. 8). Hence, the percentage of long-reads that can  
306 be assigned to their allelic origin with high confidence is reduced (Supplemental Table 2, 8).

307

308 Despite having lower depth of sequencing and fewer informative SNPs per transcript, we  
309 identified three ASM sites with reproducible and large effect sizes. These three sites were found  
310 on the *BTN3A2* (FDR=0.006), *FCMR* (FDR=0.006), and *TNFSF9* (FDR=0.47) transcripts (Fig. 5B,

311 Supplemental Fig. 9-10). All three events were observed within the 3' UTR and exhibited large  
312 differences in modification ratio between the two alleles (Fig. 5C; mean difference in modification  
313 ratio 0.657, *BTN3A2*; 0.500, *FCMR*; and 0.390, *TNFSF9*). *BTN3A2* plays a crucial role in T cell  
314 activation and proliferation (Vantourout et al. 2018; Kabelitz and Dechanet-Merville 2016), *FCMR*,  
315 which encodes the IgM Fc receptor, is vital for B cell activation and survival (Wang et al. 2016),  
316 and *TNFSF9*, a member of the TNF superfamily, enhances T cell responses by interacting with  
317 CD137 on activated T lymphocytes (Wang et al. 2016; Hashimoto 2021). The applicability of our  
318 ONT DRS method for ASM detection in human cells supports the wide-ranging utility of our  
319 approach in any system with known genetic information.

320

### 321 **RNA abundance is higher for the allele with higher m6A modification ratio**

322 Allele-specific differences in m6A modification provides a powerful platform to assess their  
323 functional impact on expression dynamics as the genetic background, environmental factors and  
324 sample preparation are identical for the two alleles. Hence, we generated matched RNA-seq and  
325 ribosome profiling data in hybrid mESCs and leveraged existing measurements for the NA12878  
326 cells (Methods) (Cenik et al. 2015). This data enabled us to determine the relative RNA expression  
327 and ribosome occupancy on each allele and correlate these with their m6A modification status.

328

329 In hybrid mESCs, transcripts harboring ASM sites demonstrated statistically significant RNA  
330 expression bias towards the allele with higher m6A modification. This pattern was consistent  
331 across both long-read and short-read sequencing methods (Fig. 6A; Binomial test p-value 0.004  
332 and 0.011, respectively). Specifically, the mean proportion of RNA reads from the CAST allele for  
333 genes exhibiting CAST-biased ASM were 0.557 and 0.558 for long-read and short-read  
334 sequencing. Similarly, genes with B6-biased ASM had higher mean proportion of RNA reads from  
335 the B6 allele (0.460 and 0.398, respectively). These observations suggest that ASM is associated  
336 with allele-specific expression in the same allelic direction.

337

338 In NA12878 cells, the association of ASM and allele-specific RNA expression was similarly  
339 evident. *BTN3A2*, possessing Allele B biased methylation site, demonstrated a high proportion of  
340 RNA reads from Allele B (mean allelic ratios 0.851 and 0.704 for long-read and short-read  
341 sequencing). Similarly, *TNFSF9* and *FCMR*, with Allele A biased methylation sites, showed  
342 slightly elevated proportions of RNA reads from the Allele A (Supplemental Fig. 11A-B). These  
343 findings further support an association with ASM and allele-specific RNA expression (Fig. 6B).

344

345 Recent studies have postulated the role of m6A modification in regulating translation (Mao et al.  
346 2019; Meyer 2019b; Jain et al. 2023). In particular, we analyzed allele-specific ribosome  
347 occupancy on genes with ASM in hybrid mESCs. We did not detect significant correlation between  
348 allele-specific ribosome occupancy and ASM (Fig. 6A; p-value, 0.83; Supplemental Fig. 11C).  
349 Collectively, our results indicate that alleles with higher m6A modification ratios are associated  
350 with increased RNA abundance but similar ribosome occupancy.

351

## 352 **DISCUSSION**

353

354 In this study, we used ONT DRS as a new method to detect allele-specific m6A RNA modifications  
355 in both human and mouse cells. Notably, the long-reads generated by the ONT approach revealed  
356 ASM sites with no nearby genetic differences, suggesting that m6A modification on a given site  
357 may depend on factors beyond local sequence context. These ASM may potentially be governed  
358 from long-range interactions that modulate mRNA secondary structure, differences in allele-  
359 specific interactions with RNA-binding proteins or the local chromatin context of each allele  
360 (Huang et al. 2019; Deng et al. 2022; Berlivet et al. 2019).

361

362 The deposition of m6A modification on mRNA is dependent on the presence of a specific motif  
363 (DRACH) surrounding the adenosine that is modified (Linder et al. 2015). Our analysis of ASM  
364 sites revealed that nucleotide identity of the positions that surround this canonical motif may also  
365 influence m6A deposition in particular contexts. Specifically, we found that alleles containing  
366 cytosine at the D-1 site followed by uracil at the D-2 site exhibit higher methylation levels  
367 (Supplemental Fig. 6).

368

369 A major strength of our approach over short-read based methods is its ability to cover many more  
370 informative SNPs to assign reads to their allelic origin (Supplemental Fig. 12, maximum SNP  
371 count per read, 12 with short-read; 78 with long-read in mESC). Hence, long-read technology has  
372 higher confidence in allelic assignment (Wu et al. 2023; Glinos et al. 2022). In contrast to short-  
373 read methods, which rely heavily on single SNPs within a read, our approach minimizes the  
374 impact of errors in genetic variant annotations by leveraging an increased number of variants.  
375 Furthermore, in samples with less genetic variation, long-reads increase the chance of linking  
376 genetic variants that may be far away from the site of interest which would not be detectable by  
377 short read based approaches.

378

379 A recent study leveraged previously generated MeRIP-seq data and claimed to detect numerous  
380 ASM sites (Cao et al. 2023). Their approach involved calculating p-values from Fisher's exact test  
381 on tables of reads per kilobase of transcript per million mapped reads for each allele from the  
382 input control and immunoprecipitation. They interpreted the resulting p-values as evidence of  
383 ASM. However, this method is fundamentally flawed. Fisher's exact test is specifically designed  
384 for categorical data and applying it to continuous data in this context is inappropriate. This misuse  
385 of the test raises serious concerns about the validity of their conclusions.

386

387 Furthermore, MeRIP-seq suffers from the additional limitations of antibody-based enrichment.  
388 Antibody-based approaches introduce specificity artifacts which result in variability in the number  
389 and location of peaks detected across experiments (Helm et al. 2019). Similarly, the  
390 immunoprecipitation step creates variable yields, limiting quantitative measurements among  
391 experiments (McIntyre et al. 2020). Therefore, the large number of sites reported by Cao et al.  
392 are inflated with a large number of false positives. In our study, we focused on large effect  
393 differences using a bootstrap resampling strategy and minimum effect size threshold to reduce  
394 statistical artifacts as previously recommended (Castel et al. 2020; Mohammadi et al. 2017).  
395 Consequently, the number of sites described here likely reflects the extent of allele-biased  
396 methylation more accurately.

397

398 To address the limitations of antibody-based detection of m6A modifications, recent work  
399 developed enzymatic and chemical approaches (Meyer 2019a; Song et al. 2021). However, the  
400 applicability of the enzymatic approach is currently restricted to a subset of m6A sites within  
401 DRACH motifs ending in ACA, constituting approximately 16% of total sites. While these  
402 advances are promising, they will likely be limited for allele-specific analysis due to the use of  
403 short read sequencing (Garcia-Campos et al. 2019).

404

405 Allelic imbalances in m6A modification ratios between transcripts can potentially lead to allele-  
406 specific RNA expression and translation based on their impact on mRNA stability, transcription  
407 and translation efficiency (Mauer et al. 2017; Cesaro et al. 2023; Min et al. 2018) Specifically,  
408 m6A reader proteins such as YTHDC1 and YTHDC2, which interact with m6A sites on 3' UTRs,  
409 enhance mRNA stability (Lee et al. 2021; Wang et al. 2014). Our study revealed a positive  
410 relationship between ASM and allele-specific RNA expression. A potential mechanism explaining  
411 this association is the allele-specific association with m6A reader proteins that subsequently  
412 stabilize m6A-enriched mRNAs.

413

414 In contrast, we did not observe an association between ASM and allele-specific ribosome  
415 occupancy. Given that ribosome occupancy is a composite measurement of RNA expression and  
416 translation efficiency (Liu et al. 2024; Zheng et al. 2024), this observation may indicate that alleles  
417 with higher modification ratios are less efficiently translated despite having higher steady-state  
418 RNA abundance. Such a mechanism would be in agreement with a previously proposed model  
419 of coupling between co-transcriptional m6A deposition and translation (Slobodin et al. 2017).

420

421 Our method has several important limitations. First, the supervised machine learning framework  
422 we adopted is predicated on the assumption that modifications occur exclusively within DRACH  
423 motifs. Consequently, our analysis does not account for genetic variations that alter the motif into  
424 sequences not matching the DRACH pattern, which are presumed to result in methylation loss.  
425 Second, the limitation in the number of reads generated by ONT DRS constrains our method's  
426 ability to detect ASM sites in lowly expressed transcripts. Hence, ASM sites identified in this study  
427 occur in genes within the top 30th percentile of RNA expression (Supplemental Fig. 4).

428

429 In summary, we present a novel method for identifying allele-specific m6A modification using ONT  
430 DRS. Our analyses emphasize the benefits of long-read sequencing and direct detection of RNA  
431 modifications for ASM analysis. Future ASM studies are likely to extend the catalog of allelic  
432 variants that influence RNA modifications, and characterize the mechanisms leading to ASM and  
433 its functional consequences on gene expression.

434

## 435 **METHODS**

436

### 437 **Cell culture**

438 The C57BL/6J-CAST/EiJ F1 Hybrid mESCs were generously provided by Dr. David Spector. Cells  
439 were cultured in 2i medium as followed the original cell culture method (Balasooriya and Spector  
440 2022).

441

#### 442 **Generation of *Mettl3* knockout mESCs**

443 *Mettl3* knockout cells were generated by introducing Cas9/sgRNA ribonucleoprotein (RNP)  
444 complexes into mESCs via nucleofection (Kirton et al. 2013). The sgRNA was synthesized by  
445 Synthego (Supplemental Table 2). To form the RNP, 300 pmol of Cas9 protein (NEB, Cat. No.  
446 M0386M) and 600 pmol of sgRNA were incubated in Cas9 Buffer (150 mM KCl, 1 mM MgCl<sub>2</sub>, 10%  
447 v/v Glycerol, 20 mM HEPES–KOH [pH 7.5]) at room temperature for 30 minutes. Subsequently,  
448 65 µL of 4D-Nucleofector X Solution was added to the RNP solution. Nucleofection was performed  
449 using the optimized protocol recommended by the manufacturer (SF Cell Line 4D-Nucleofector™  
450 X Kit L). A cell pellet was collected from  $2 \times 10^6$  cells, resuspended in the RNP solution, and  
451 transferred into a 100 µL Nucleocuvette Vessel. Electroporation was carried out using the 4D-  
452 Nucleofector X Unit (Lonza) with the FF120 program. Post-nucleofection, cells were equilibrated  
453 at room temperature for 8 minutes, then transferred to a gelatin coated culture dish containing  
454 prewarmed 2i media. The cells were allowed to recover at 37 °C for 72 hours, followed by the  
455 isolation of single clones using serial dilution. The genomic DNA was isolated from cells grown  
456 from single clones and mutations were confirmed using the primers listed in Supplemental Table  
457 2.

458

#### 459 **ONT DRS**

460 mESCs were collected from two different numbers of passages on separate days, and considered  
461 as two biological replicates. The cells were lysed in TRIzol reagent (Zymo Research, Cat. No.  
462 R2050) and RNA was extracted according to the manufacturer's instructions (Zymo Direct-zol  
463 RNA Kits, Cat. No. R2061). 5 µg of total RNA without poly(A) RNA isolation was used for direct

464 RNA sequencing (Viscardi and Arribere 2022). The library was generated using the Oxford  
465 Nanopore Direct RNA Sequencing Kit (Nanopore Cat. No. SQK-RNA002) following the  
466 manufacturer's protocol. The RNA sequencing from each RNA replicate was performed on four  
467 MinION Mk1b with R9.4 flow cells (Oxford Nanopore Technologies Ltd.) with a 24-h runtime for  
468 each run.

469  
470 We utilized published ONT DRS data from the human cell line NA12878 downloaded from  
471 <https://github.com/nanopore-wgs-consortium/NA12878> (Hansen 2016; Workman et al. 2018).  
472 Raw FAST5 files were used directly for analysis.

473

#### 474 **m6A detection from ONT DRS**

475 Guppy v. 6.3.2 (Wick et al. 2019) (quality score cutoff = 7) was used for base-calling from FAST5  
476 files, and error rates were analyzed with Pomoxis v0.3.15 (Buttler and Drown 2022). Reads were  
477 aligned to the transcriptome with minimap 2.1 '-ax map-ont' option (Li 2018). To reduce alignment  
478 biases, we used a transcriptome reference in which SNPs were masked with Ns as previously  
479 described (Ozadam et al. 2023). A mouse VCF was downloaded from the Mouse Genome Project  
480 (<https://www.mousegenomes.org/>), and the NA12878 VCF file was obtained from  
481 <https://hgdownload.soe.ucsc.edu/gbdb/hg38/platinumGenomes/>.

482

483 To identify m6A modifications, we used Nanopolish v0.11.3 (Loman et al. 2015) to generate an  
484 index with the '--scale-events' and '--signal-index' options, aligning events to the N-masked  
485 transcriptome reference. Detection of m6A RNA modifications was conducted using m6Anet v-  
486 2.0.0 and a pretrained model (Hct116\_RNA002) (Hendra et al. 2022). A minimum of 20 reads per  
487 site was required to call modification sites.

488

#### 489 **Assignment of reads to their allelic origin**

490 To assign aligned reads to their allelic origin, we identified the positions on each read that  
491 correspond to a SNP, adjusting for any deletions and insertions in the read with respect to the  
492 reference. The number of heterozygous SNPs in mESC and NA12878 transcriptomes was  
493 210,004, and 27,269, respectively (Supplemental Fig. 8). Consequently, we required at least three  
494 SNPs per read for mESCs, and one SNP for NA12878. Then, we calculated the number of  
495 matches to each allele and defined a read-level allele-bias ratio:

$$496 \quad \textit{Allele A bias ratio} = \frac{\textit{SNP count from Allele A in a read}}{\textit{total number of detected SNPs in a read}}$$

497  
498 We assigned each read into one of three groups based on this ratio: allele A (bias ratio exceeding  
499 0.7), allele B (bias ratio less than 0.3), and undefined (bias ratio between 0.3 and 0.7). The  
500 process was implemented in a Python script that is provided on GitHub: `allele_assignment.py`.  
501 Subsequently, the three groups of reads underwent processing through m6Anet separately to  
502 predict m6A probability and modification ratios as described above.

503

#### 504 **Identification of allele-specific m6A modifications**

505 We first selected m6A sites with a high probability of modification ( $\text{prob} > 0.85$ ) using all reads.  
506 When the SNPs on the motif convert DRACH motifs to non-DRACH motifs, we exclude them from  
507 the analysis because non-DRACH motifs are by definition assumed to be unmethylated (Hendra  
508 et al. 2022). In mESCs, 29 SNP overlapping the motif led to different instances of the DRACH  
509 sequences among a total of 178 and 145 sites, respectively (Supplemental Fig. 13). In NA12878,  
510 the corresponding numbers were 1 in 5 (JHU), 1 in 11 (OICR), 1 in 21 (UBC), 2 in 24 (UCSC), 2  
511 in 22 (UN).

512

513 If both alleles had more than 20 reads, the modification ratios were used directly as calculated by  
514 m6Anet (63% of total). However, when one of the two alleles has a read count less than 20, we

515 recalculated the modification ratio leveraging modification information from all reads, without  
 516 distinguishing the two alleles. Without loss of generality, let's assume that allele A had fewer than  
 517 20 reads assigned and hence was not considered by m6Anet. In this case, we first calculated its  
 518 read count by following:

$$519 \quad \textit{Allele A read count} = \textit{Total read counts} - \textit{Allele B read counts} - \textit{Undefined read counts}$$

520

521 If at least 10 reads were assigned to allele A, we retained this site for further analysis and  
 522 recalculated the modification ratio of allele A using the following formula:

523 *Allele A mod ratio*

$$524 \quad = \frac{(\textit{Total read count} \times \textit{mod ratio from total reads}) - (\textit{Allele B read count} \times \textit{Allele B mod ratio})}{\textit{Allele A read count}}$$

525 See Supplemental Fig. 14 for a schematic description of this procedure.

526

527 We identified statistically significant ASM sites using a bootstrapping-based statistical test. First,  
 528 for each allele, methylated read counts were derived by multiplying modification ratios with total  
 529 read numbers. We then sampled the number of methylated reads for each allele with replacement  
 530 and calculated the difference between the modification ratios using the resampled read counts  
 531 (McLachlan and Rathnayake 2014; Banjanovic and Osborne 2016). This resampling procedure  
 532 was repeated 1,000,000 times and a one-sided p-value was calculated by using a effect size  
 533 threshold ( $T$ ) of 0 or 0.1 as follows:

$$534 \quad p \textit{ value} = 1 - \frac{|\{b: (\textit{Mod Ratio}_b^A - \textit{Mod Ratio}_b^B) > (T)\}|}{1,000,000}$$

535 where,  $\textit{Mod Ratio}_b^A$  represents the bootstrap resampling value for the allele with the higher  
 536 observed m6A modification ratio. An aggregate p-value was calculated by combining the p-values  
 537 from each replicate using the harmonic mean method (Wilson 2019). False Discovery Rate (FDR)  
 538 was calculated by the Benjamini & Hochberg method (Yoav Benjamini 1995). Finally, statistically

539 significant ASM sites were defined if adjusted harmonic mean p-values (FDR) were below 0.1.  
 540 For instance, with an effect size threshold of 0.1 ( $T = 0.1$ ), if none of the randomizations exceed  
 541 this cutoff, it would suggest that the modification ratios of the two alleles from resampled reads  
 542 are highly similar. Consequently, the probability of this site being an ASM would be very low,  
 543 corresponding to a p-value of 1.

544  
 545 To assess the significance of UGACU being the most common DRACH variant among Group 2  
 546 ASM sites, we randomly resampled 17 motifs 10,000 times. For the resampling, we used the  
 547 observed frequency of each of the 15 instances of the DRACH motif among sites with a high  
 548 probability of modification. In these random samples, only 84 instances had UGACU as the most  
 549 frequent motif hence corresponding to a p-value of 0.0084.

550

#### 551 **mESC MeRIP-seq experiments and analyses**

552 MeRIP-seq libraries were prepared with EpiNext CUT&RUN RNA m6A-Seq Kit (EpiGentek). The  
 553 three replicates of mESCs were collected from different numbers of passages on separate dates.  
 554 The total RNA was extracted with Direct-zol RNA Purification Kits (Zymo Research, Cat. No.  
 555 R2050). 7  $\mu$ g of total RNA was subjected to immunoprecipitation with an m6A antibody (P9016,  
 556 EpiGentek, 1:100 dilution) and digested with cleavage enzyme on beads. The beads were then  
 557 washed three times with a wash buffer and protein digestion buffer, and RNA was eluted in 13  $\mu$ l  
 558 of the elution buffer. The sequencing libraries were generated using the Diagenode small RNA  
 559 sequencing kit (Diagenode, Cat. No. C05030001). The libraries were sequenced on a  
 560 NovaSeq6000 system (Illumina).

561  
 562 Adaptor sequences were trimmed from raw reads with cutadapt v4.7 (Martin 2011) using following

563 parameters: `-a AAAAAAAAAACAAAAAAAAA -G ^TTTTTTTTTGTTTTTTTTTT -A`  
 564 `AGATCGGAAGAGCGTCGTGTAGGGAAAGAGTGT -n 2 --overlap=4 --trimmed-only --maximum-`

565 length=150 --minimum-length=31 --quality-cutoff=28. Trimmed reads were aligned to the N-masked  
566 mouse transcriptome with STAR v2.7.10b (Dobin et al. 2013). Reads with low mapping quality  
567 were discarded (mapping quality <10) and indexed with SAMtools v1.15.1 (Danecek et al. 2021;  
568 Bonfield et al. 2021).

569

570 To compute the allele bias ratio, we counted the number of allelic reads that harbor at least one  
571 SNP within 100 bp of the ASM sites. Out of 23 ASM sites, four did not have genetic differences  
572 within 100 base pairs of the methylated position and 15 had fewer than 40 reads across the three  
573 replicates (Supplemental Table 6). Allele bias for the remaining four sites were calculated as:

$$574 \quad \textit{Allele bias ratio} = \frac{\textit{CAST allele read count}}{\textit{B6 allele read count} + \textit{CAST allele read count}}$$

575

#### 576 **mESC RNA-seq and ribosome profiling library preparation**

577 Five million mESCs were scraped and transferred to 1.5 mL tubes in iced lysis buffer (20 mM Tris  
578 HCl pH 7.4, 150 mM NaCl, 5 mM MgCl<sub>2</sub>, 1 mM DTT, 100 µg/mL Cycloheximide, 1% Triton-X).  
579 The lysate was clarified by centrifugation at 1300 × g for 10 min at 4 °C. 10% of the clarified lysate  
580 by volume was reserved for RNA extraction using Direct-zol RNA Purification Kits (Zymo  
581 Research, Cat. No. R2050). The RNA-seq libraries were prepared using the NEBNext Ultra™ II  
582 RNA Library Prep Kit.

583

584 7 µL of RNaseI (Invitrogen, Cat. No. AM2249) was added to the remaining lysate for ribosome  
585 profiling (following REF with minor modifications) (Rao et al. 2021). Digestion was carried out for  
586 1 h at 4 °C, and stopped with ribonucleoside vanadyl complex (NEB, Cat. No. S1402S) at a final  
587 concentration of 20 mM. Digested lysates were layered on a sucrose cushion (20 mM Tris HCl  
588 pH 7.4, 150 mM NaCl, 5 mM MgCl<sub>2</sub>, 34% sucrose, 1 mM DTT) and the ribosomes were pelleted  
589 by centrifugation in a SW 41 Ti rotor (Beckman Coulter) at 38,000 rpm for 2.5 h at 4°C. RNA was

590 isolated with the RNeasy Mini RNA Kit (Qiagen, Cat. No. 74104) and size-selected by running 5  
591  $\mu\text{g}$  of each sample on a 15% polyacrylamide TBE-UREA gel. The 21–34 nt RNA fragments were  
592 excised and extracted by crushing the gel fragment in the RNA extraction buffer (300 mM sodium  
593 acetate pH 5.5, 1 mM EDTA, 0.25% SDS) followed by an overnight incubation at room  
594 temperature. The sample was passed through a Spin X filter (Corning, Cat. No. 8160) and the  
595 flowthrough was ethanol precipitated in the presence of 5 mM  $\text{MgCl}_2$  and 1  $\mu\text{L}$  GlycoBlue  
596 (Invitrogen, Cat. No. AM9516). The RNA pellet was resuspended in 10  $\mu\text{L}$  of RNase-free water  
597 and immediately processed for library preparation using D-Plex Small RNA-seq kit (Diagenode,  
598 Cat. No. C05030001) with slight modifications. The dephosphorylation reaction was  
599 supplemented with 0.5  $\mu\text{l}$  T4 PNK (NEB, Cat. No. M0201S), and the reaction was incubated for  
600 25 minutes. Subsequently, the complementary DNA (cDNA) was amplified for 12 PCR cycles.  
601 We used AMPure XP bead cleanup (1.8X), followed by size selection using 3% agarose, dye-free  
602 gel cassettes with internal standards (Sage Science, Cat. No. BDQ3010) on the BluePippin  
603 platform. Sequencing was performed on a NovaSeq 6000 platform.

604

### 605 **Read processing of RNA-seq and ribosome profiling**

606 For mESC, RNA-seq and Ribo-seq data were processed using RiboFlow v0.0.1 (Ozadam et al.  
607 2020). For the Ribo-seq library, Unique Molecular Identifier (UMI) sequences were isolated  
608 employing the following parameters: "umi\_tools extract -p  
609 '^(?P<umi\_1>.{12})(?P<discard\_1>.{4}).+\${' --extract-method=regex". Subsequently, reads  
610 underwent clipping with the parameters "-a AAAAAAAAAACAAAAAAAAA --overlap=4 --trimmed-  
611 only". Trimmed reads were then filtered by alignment to mouse rRNA and tRNA sequences with  
612 Bowtie2 v 7.3.0 (Langmead and Salzberg 2012), and utilizing unaligned reads for subsequent  
613 alignment to the N-masked transcriptome. Following transcriptome alignment, reads (mapping  
614 quality > 2) were preserved and deduplicated utilizing UMI-tools (Smith et al. 2017) directional  
615 adjacency method with the parameter "--read-length".

616

617 In mESC RNA-seq analysis, we clipped read adaptors using cutadapt, v1.18 (Martin 2011) “-a  
618 AGATCGGAAGAGCACACGTCTGAACTCCAGTCA -A AGATCGGAAGAGCGTCGTGTAGGGAAAGAGTGT -O  
619 8 -m 20 --cores=8”. The reads were aligned to the N-masked transcriptome, and the read count  
620 for RNA-seq and Ribo-seq were obtained from .ribo files with RiboR (Ozadam et al. 2020). Quality  
621 control metrics were inspected using RiboR and RiboGraph (Chacko et al. 2024).

622

623 For the NA12878 sample, we analyzed RNA-seq and Ribo-seq data (NCBI Gene Expression  
624 Omnibus (GEO) under accession number GSE65912) based on the study by Cenik et al. (Cenik  
625 et al. 2015). We trimmed read NEB adaptors using the same option that we used for mESC RNA-  
626 seq, then filtered by aligning to human rRNA and tRNA sequences with Bowtie2 v7.3.0. Unaligned  
627 reads were subsequently mapped to the N-masked human transcriptome.

628

### 629 **Allele-specific RNA expression and ribosome occupancy analysis**

630 Utilizing the aligned BAM files obtained from RNA-seq and Ribo-seq, ASE counts were acquired  
631 using GATK v3.8.1 ASEReadCounter (McKenna et al. 2010). The fraction of reads corresponding  
632 to the two alleles was calculated for all loci. After normalization by count per million reads, ASE  
633 scores were computed by dividing the read count from a certain allele to the sum of the read  
634 counts from both alleles (Castel et al. 2015; Liu et al. 2018).

635

636 To compare the allele-specific RNA expression and ribosome occupancy ratio in genes which  
637 have ASM, we obtained allele bias ratio to the same allele (e.g., allele A) which showed ASM  
638 (e.g., allele A bias methylation).

639

$$\text{Allele A bias ratio} = \frac{\text{Allele A read count}}{\text{Allele A read count} + \text{Allele B read count}}$$

640

641 To quantify the relationship between the allele-bias ratio from long-read sequencing and short-  
642 read sequencing, we calculate the weighted rho using long-read sequencing read counts as  
643 weights. The correlation was calculated by using R package “boot”, v1.3-30 (Davison and Hinkley  
644 1997).

645

#### 646 **Genomic DNA extraction and PCR for genetic variant verification**

647 Genomic DNA from mESCs was extracted using the Quick-DNA Miniprep Plus Kit (Zymo, Cat.  
648 No. D4068). The target regions were amplified by PCR using Q5 High-Fidelity DNA Polymerase  
649 (NEB, Cat. No. M0491S) using 17 primer pairs (Supplemental Table 9). The resulting PCR  
650 products were purified using the NucleoSpin Gel and PCR Clean-up Kit (Takara, Cat. No.  
651 740609.250) and sequenced by Sanger sequencing (ACGT, Inc. DNA sequencing service).

652

#### 653 **DATA ACCESS**

654 All mESC short-read sequencing data sets and the base-called DRS data presented in this paper  
655 have been deposited in the Sequence Read Archive under BioProject accession number  
656 PRJNA1071025 (SRP486746). The ONT DRS data is available on Zenodo under the following  
657 record numbers: mESC replicate 1 (10815502, 13255832, 13256383), mESC replicate 2  
658 (13257639, 13259594, 13273847, 13275906, 13278114, 13277067), and Mettl3 knockout cells  
659 (13257082). All custom scripts used to perform bioinformatics analyses available on GitHub:  
660 <https://github.com/DayeaPark/Allele-specific-m6A-modification.git>

661

#### 662 **COMPETING INTEREST STATEMENT**

663 We declare no competing interests.

664

665 **ACKNOWLEDGMENTS**

666 We thank Dr. David Spector for kindly providing hybrid mESCs. We appreciate the insightful  
667 comments provided by Dr. Ian Hoskins on the manuscript. This work was supported by National  
668 Institutes of Health grants [HD110096, GM150667], as well as a Welch Foundation grant [F-2027-  
669 20230405] (C.C.). Figures were generated using BioRender.com under a publication license  
670 (JO26GB978U). All original text in this paper was authored by the researchers. Additionally, we  
671 acknowledge the assistance of a Large Language Model (OpenAI, ChatGPT v3.5) for suggesting  
672 edits aimed at improving clarity and grammar.

673

674 *Author contributions:* Conceptualization, Methodology, Investigation, Formal analysis,  
675 Visualization, and Writing- Original Draft (D.P.) Funding acquisition, Project administration, and  
676 Supervision (C.C.) Editing and Review (C.C and D.P.)

677

678 **REFERENCES**

- 679 Akhtar J, Lugoboni M, Junion G. 2021. m6A RNA modification in transcription regulation.  
680 *Transcription* **12**: 266–276.
- 681 Amoah K, Hsiao Y-HE, Bahn JH, Sun Y, Burghard C, Tan BX, Yang E-W, Xiao X. 2021. Allele-  
682 specific alternative splicing and its functional genetic variants in human tissues. *Genome*  
683 *Res* **31**: 359–371.
- 684 Balasooriya GI, Spector DL. 2022. Allele-specific differential regulation of monoallelically  
685 expressed autosomal genes in the cardiac lineage. *Nat Commun* **13**: 5984.
- 686 Banjanovic ES, Osborne JW. 2016. Confidence intervals for effect sizes: Applying bootstrap  
687 resampling. *Practical Assessment, Research, and Evaluation*.  
688 <https://openpublishing.library.umass.edu/pare/article/id/1604/>.
- 689 Berlivet S, Scutenaire J, Deragon J-M, Bousquet-Antonelli C. 2019. Readers of the mA  
690 epitranscriptomic code. *Biochim Biophys Acta Gene Regul Mech* **1862**: 329–342.
- 691 Bokar JA, Rath-Shambaugh ME, Ludwiczak R, Narayan P, Rottman F. 1994. Characterization  
692 and partial purification of mRNA N6-adenosine methyltransferase from HeLa cell nuclei.  
693 Internal mRNA methylation requires a multisubunit complex. *J Biol Chem* **269**: 17697–  
694 17704.
- 695 Bonfield JK, Marshall J, Danecek P, Li H, Ohan V, Whitwham A, Keane T, Davies RM. 2021.  
696 HTSlib: C library for reading/writing high-throughput sequencing data. *Gigascience* **10**.  
697 <http://dx.doi.org/10.1093/gigascience/giab007>.
- 698 Buttler J, Drown DM. 2022. Accuracy and Completeness of Long Read Metagenomic  
699 Assemblies. *Microorganisms* **11**. <http://dx.doi.org/10.3390/microorganisms11010096>.
- 700 Cao S, Zhu H, Cui J, Liu S, Li Y, Shi J, Mo J, Wang Z, Wang H, Hu J, et al. 2023. Allele-specific  
701 RNA N 6-methyladenosine modifications reveal functional genetic variants in human  
702 tissues. *Genome Res* **33**: 1369–1380.
- 703 Castel SE, Aguet F, Mohammadi P, GTEx Consortium, Ardlie KG, Lappalainen T. 2020. A vast  
704 resource of allelic expression data spanning human tissues. *Genome Biol* **21**: 234.
- 705 Castel SE, Levy-Moonshine A, Mohammadi P, Banks E, Lappalainen T. 2015. Tools and best  
706 practices for data processing in allelic expression analysis. *Genome Biol* **16**: 195.
- 707 Cenik C, Cenik ES, Byeon GW, Grubert F, Candille SI, Spacek D, Alsallakh B, Tilgner H, Araya  
708 CL, Tang H, et al. 2015. Integrative analysis of RNA, translation, and protein levels reveals  
709 distinct regulatory variation across humans. *Genome Res* **25**: 1610–1621.
- 710 Cenik C, Chua HN, Singh G, Akef A, Snyder MP, Palazzo AF, Moore MJ, Roth FP. 2017. A  
711 common class of transcripts with 5'-intron depletion, distinct early coding sequence  
712 features, and N1-methyladenosine modification. *RNA* **23**: 270–283.
- 713 Cesaro B, Tarullo M, Fatica A. 2023. Regulation of Gene Expression by m6Am RNA  
714 Modification. *Int J Mol Sci* **24**. <http://dx.doi.org/10.3390/ijms24032277>.

- 715 Chacko J, Ozadam H, Cenik C. 2024. RiboGraph: an interactive visualization system for  
716 ribosome profiling data at read length resolution. *Bioinformatics* **40**.  
717 <http://dx.doi.org/10.1093/bioinformatics/btae369>.
- 718 Chen K, Luo G-Z, He C. 2015. High-Resolution Mapping of N<sup>6</sup>-Methyladenosine in  
719 Transcriptome and Genome Using a Photo-Crosslinking-Assisted Strategy. *Methods*  
720 *Enzymol* **560**: 161–185.
- 721 Chen Z, Lei C, Wang C, Li N, Srivastava M, Tang M, Zhang H, Choi JM, Jung SY, Qin J, et al.  
722 2019. Global phosphoproteomic analysis reveals ARMC10 as an AMPK substrate that  
723 regulates mitochondrial dynamics. *Nat Commun* **10**: 104.
- 724 Cho H, Davis J, Li X, Smith KS, Battle A, Montgomery SB. 2014. High-resolution transcriptome  
725 analysis with long-read RNA sequencing. *PLoS One* **9**: e108095.
- 726 Danecek P, Bonfield JK, Liddle J, Marshall J, Ohan V, Pollard MO, Whitwham A, Keane T,  
727 McCarthy SA, Davies RM, et al. 2021. Twelve years of SAMtools and BCFtools.  
728 *Gigascience* **10**. <http://dx.doi.org/10.1093/gigascience/giab008>.
- 729 David J. Adams, Anthony G. Doran, Jingtao Lilue & Thomas M. Keane. 2015. The Mouse  
730 Genomes Project: a repository of inbred laboratory mouse strain genomes. *Mamm Genome*  
731 **26**: 403–412.
- 732 Davison AC, Hinkley DV. 1997. *Bootstrap Methods and Their Application*. Cambridge University  
733 Press.
- 734 de la Chapelle A. 2009. Genetic predisposition to human disease: allele-specific expression and  
735 low-penetrance regulatory loci. *Oncogene* **28**: 3345–3348.
- 736 Deng S, Zhang J, Su J, Zuo Z, Zeng L, Liu K, Zheng Y, Huang X, Bai R, Zhuang L, et al. 2022.  
737 RNA m<sup>6</sup>A regulates transcription via DNA demethylation and chromatin accessibility. *Nat*  
738 *Genet* **54**: 1427–1437.
- 739 DeVeale B, van der Kooy D, Babak T. 2012. Critical Evaluation of Imprinted Gene Expression  
740 by RNA–Seq: A New Perspective. *PLoS Genet* **8**: e1002600.
- 741 Dobin A, Davis CA, Schlesinger F, Drenkow J, Zaleski C, Jha S, Batut P, Chaisson M, Gingeras  
742 TR. 2013. STAR: ultrafast universal RNA-seq aligner. *Bioinformatics* **29**: 15–21.
- 743 Dominissini D, Moshitch-Moshkovitz S, Schwartz S, Salmon-Divon M, Ungar L, Osenberg S,  
744 Cesarkas K, Jacob-Hirsch J, Amariglio N, Kupiec M, et al. 2012. Topology of the human  
745 and mouse m<sup>6</sup>A RNA methylomes revealed by m<sup>6</sup>A-seq. *Nature* **485**: 201–206.
- 746 Fan J, Hu J, Xue C, Zhang H, Susztak K, Reilly MP, Xiao R, Li M. 2020. ASEP: Gene-based  
747 detection of allele-specific expression across individuals in a population by RNA  
748 sequencing. *PLoS Genet* **16**: e1008786.
- 749 Fournier C, Goto Y, Ballestar E, Delaval K, Hever AM, Esteller M, Feil R. 2002. Allele-specific  
750 histone lysine methylation marks regulatory regions at imprinted mouse genes. *EMBO J* **21**:  
751 6560–6570.
- 752 Garalde DR, Snell EA, Jachimowicz D, Sipos B, Lloyd JH, Bruce M, Pantic N, Admassu T,  
753 James P, Warland A, et al. 2018. Highly parallel direct RNA sequencing on an array of

- 754       nanopores. *Nat Methods* **15**: 201–206.
- 755       Garcia-Campos MA, Edelheit S, Toth U, Safra M, Shachar R, Viukov S, Winkler R, Nir R,  
756       Lasman L, Brandis A, et al. 2019. Deciphering the “m6A Code” via Antibody-Independent  
757       Quantitative Profiling. *Cell* **178**: 731–747.e16.
- 758       Gicquel C, Rossignol S, Cabrol S, Houang M, Steunou V, Barbu V, Danton F, Thibaud N, Le  
759       Merrer M, Burglen L, et al. 2005. Epimutation of the telomeric imprinting center region on  
760       chromosome 11p15 in Silver-Russell syndrome. *Nat Genet* **37**: 1003–1007.
- 761       Glinos DA, Garborcauskas G, Hoffman P, Ehsan N, Jiang L, Gokden A, Dai X, Aguet F, Brown  
762       KL, Garimella K, et al. 2022. Transcriptome variation in human tissues revealed by long-  
763       read sequencing. *Nature* **608**: 353–359.
- 764       Hansen NF. 2016. Variant Calling From Next Generation Sequence Data. In *Statistical*  
765       *Genomics: Methods and Protocols* (eds. E. Mathé and S. Davis), pp. 209–224, Springer  
766       New York, New York, NY.
- 767       Hashimoto K. 2021. CD137 as an Attractive T Cell Co-Stimulatory Target in the TNFRSF for  
768       Immuno-Oncology Drug Development. *Cancers* **13**.  
769       <http://dx.doi.org/10.3390/cancers13102288>.
- 770       Helm M, Lyko F, Motorin Y. 2019. Limited antibody specificity compromises epitranscriptomic  
771       analyses. *Nat Commun* **10**: 5669.
- 772       Hendra C, Pratanwanich PN, Wan YK, Goh WSS, Thiery A, Göke J. 2022. Detection of m6A  
773       from direct RNA sequencing using a multiple instance learning framework. *Nat Methods* **19**:  
774       1590–1598.
- 775       He PC, He C. 2021. m6A RNA methylation: from mechanisms to therapeutic potential. *EMBO J*  
776       **40**: e105977.
- 777       He PC, Wei J, Dou X, Harada BT, Zhang Z, Ge R, Liu C, Zhang L-S, Yu X, Wang S, et al. 2023.  
778       Exon architecture controls mRNA m6A suppression and gene expression. *Science* **379**:  
779       677–682.
- 780       Huang H, Weng H, Zhou K, Wu T, Zhao BS, Sun M, Chen Z, Deng X, Xiao G, Auer F, et al.  
781       2019. Histone H3 trimethylation at lysine 36 guides m6A RNA modification co-  
782       transcriptionally. *Nature* **567**: 414–419.
- 783       Jain S, Koziej L, Poulis P, Kaczmarczyk I, Gaik M, Rawski M, Ranjan N, Glatt S, Rodnina MV.  
784       2023. Modulation of translational decoding by m6A modification of mRNA. *Nat Commun* **14**:  
785       4784.
- 786       Jiang X, Liu B, Nie Z, Duan L, Xiong Q, Jin Z, Yang C, Chen Y. 2021. The role of m6A  
787       modification in the biological functions and diseases. *Signal Transduct Target Ther* **6**: 74.
- 788       Joglekar A, Prjibelski A, Mahfouz A, Collier P, Lin S, Schlusche AK, Marrocco J, Williams SR,  
789       Haase B, Hayes A, et al. 2021. A spatially resolved brain region- and cell type-specific  
790       isoform atlas of the postnatal mouse brain. *Nat Commun* **12**: 463.
- 791       Kabelitz D, Dechanet-Merville J. 2016. *Recent Advances in  $\gamma\delta$  T Cell Biology: New Ligands,*  
792       *New Functions, and New Translational Perspectives*. Frontiers Media SA.

- 793 Kirton HM, Pettinger L, Gamper N. 2013. Transient Overexpression of Genes in Neurons Using  
794 Nucleofection. In *Ion Channels: Methods and Protocols* (ed. N. Gamper), pp. 55–64,  
795 Humana Press, Totowa, NJ.
- 796 Langmead B, Salzberg SL. 2012. Fast gapped-read alignment with Bowtie 2. *Nat Methods* **9**:  
797 357–359.
- 798 Lee J-H, Wang R, Xiong F, Krakowiak J, Liao Z, Nguyen PT, Moroz-Omori EV, Shao J, Zhu X,  
799 Bolt MJ, et al. 2021. Enhancer RNA m6A methylation facilitates transcriptional condensate  
800 formation and gene activation. *Mol Cell* **81**: 3368–3385.e9.
- 801 Lee Y, Choe J, Park OH, Kim YK. 2020. Molecular Mechanisms Driving mRNA Degradation by  
802 m6A Modification. *Trends Genet* **36**: 177–188.
- 803 Li H. 2018. Minimap2: pairwise alignment for nucleotide sequences. *Bioinformatics* **34**: 3094–  
804 3100.
- 805 Linder B, Grozhik AV, Olarerin-George AO, Meydan C, Mason CE, Jaffrey SR. 2015. Single-  
806 nucleotide-resolution mapping of m6A and m6Am throughout the transcriptome. *Nat*  
807 *Methods* **12**: 767–772.
- 808 Lin S, Gregory RI. 2014. Methyltransferases modulate RNA stability in embryonic stem cells.  
809 *Nat Cell Biol* **16**: 129–131.
- 810 Liu H, Begik O, Lucas MC, Ramirez JM, Mason CE, Wiener D, Schwartz S, Mattick JS, Smith  
811 MA, Novoa EM. 2019. Accurate detection of m6A RNA modifications in native RNA  
812 sequences. *Nat Commun* **10**: 4079.
- 813 Liu J, Yue Y, Han D, Wang X, Fu Y, Zhang L, Jia G, Yu M, Lu Z, Deng X, et al. 2013. A  
814 METTL3–METTL14 complex mediates mammalian nuclear RNA N6-adenosine  
815 methylation. *Nat Chem Biol* **10**: 93–95.
- 816 Liu Y, Hoskins I, Geng M, Zhao Q, Chacko J, Qi K, Persyn L, Wang J, Zheng D, Zhong Y, et al.  
817 2024. Translation efficiency covariation across cell types is a conserved organizing  
818 principle of mammalian transcriptomes. *bioRxiv*.  
819 <http://dx.doi.org/10.1101/2024.08.11.607360>.
- 820 Liu Z, Dong X, Li Y. 2018. A Genome-Wide Study of Allele-Specific Expression in Colorectal  
821 Cancer. *Front Genet* **9**: 570.
- 822 Loman NJ, Quick J, Simpson JT. 2015. A complete bacterial genome assembled de novo using  
823 only nanopore sequencing data. *Nat Methods* **12**: 733–735.
- 824 Mao Y, Dong L, Liu X-M, Guo J, Ma H, Shen B, Qian S-B. 2019. mA in mRNA coding regions  
825 promotes translation via the RNA helicase-containing YTHDC2. *Nat Commun* **10**: 5332.
- 826 Martin M. 2011. Cutadapt removes adapter sequences from high-throughput sequencing reads.  
827 *EMBnet journal*. <http://journal.embnet.org/index.php/embnetjournal/article/view/200>.
- 828 Mauer J, Luo X, Blanjoie A, Jiao X, Grozhik AV, Patil DP, Linder B, Pickering BF, Vasseur J-J,  
829 Chen Q, et al. 2017. Reversible methylation of mA in the 5' cap controls mRNA stability.  
830 *Nature* **541**: 371–375.

- 831 McIntyre ABR, Gokhale NS, Cerchiatti L, Jaffrey SR, Horner SM, Mason CE. 2020. Limits in the  
832 detection of m6A changes using MeRIP/m6A-seq. *Sci Rep* **10**: 6590.
- 833 McKenna A, Hanna M, Banks E, Sivachenko A, Cibulskis K, Kernytzky A, Garimella K, Altshuler  
834 D, Gabriel S, Daly M, et al. 2010. The Genome Analysis Toolkit: a MapReduce framework  
835 for analyzing next-generation DNA sequencing data. *Genome Res* **20**: 1297–1303.
- 836 McLachlan GJ, Rathnayake S. 2014. On the number of components in a Gaussian mixture  
837 model. *Wiley Interdiscip Rev Data Min Knowl Discov* **4**: 341–355.
- 838 Meyer KD. 2019a. DART-seq: an antibody-free method for global m6A detection. *Nat Methods*  
839 **16**: 1275–1280.
- 840 Meyer KD. 2019b. m6A-mediated translation regulation. *Biochim Biophys Acta Gene Regul*  
841 *Mech* **1862**: 301–309.
- 842 Meyer KD, Saletore Y, Zumbo P, Elemento O, Mason CE, Jaffrey SR. 2012. Comprehensive  
843 analysis of mRNA methylation reveals enrichment in 3' UTRs and near stop codons. *Cell*  
844 **149**: 1635–1646.
- 845 Min K-W, Zealy RW, Davila S, Fomin M, Cummings JC, Makowsky D, Mcdowell CH, Thigpen H,  
846 Hafner M, Kwon S-H, et al. 2018. Profiling of m6A RNA modifications identified an age-  
847 associated regulation of AGO2 mRNA stability. *Aging Cell* **17**: e12753.
- 848 Mohammadi P, Castel SE, Brown AA, Lappalainen T. 2017. Quantifying the regulatory effect  
849 size of cis-acting genetic variation using allelic fold change. *Genome Res* **27**: 1872–1884.
- 850 Nembaware V, Lupindo B, Schouest K, Spillane C, Scheffler K, Seoighe C. 2008. Genome-wide  
851 survey of allele-specific splicing in humans. *BMC Genomics* **9**: 265.
- 852 Ozadam H, Geng M, Cenik C. 2020. RiboFlow, RiboR and RiboPy: an ecosystem for analyzing  
853 ribosome profiling data at read length resolution. *Bioinformatics* **36**: 2929–2931.
- 854 Ozadam H, Tonn T, Han CM, Segura A, Hoskins I, Rao S, Ghatpande V, Tran D, Catoe D, Salit  
855 M, et al. 2023. Single-cell quantification of ribosome occupancy in early mouse  
856 development. *Nature* **618**: 1057–1064.
- 857 Pai AA, Cain CE, Mizrahi-Man O, De Leon S, Lewellen N, Veyrieras J-B, Degner JF, Gaffney  
858 DJ, Pickrell JK, Stephens M, et al. 2012. The contribution of RNA decay quantitative trait  
859 loci to inter-individual variation in steady-state gene expression levels. *PLoS Genet* **8**:  
860 e1003000.
- 861 Pelizzola M, Baranov PV, Dassi E. 2021. *Computational Epitranscriptomics: Bioinformatic*  
862 *Approaches for the Analysis of RNA Modifications*. Frontiers Media SA.
- 863 Piccolo SR, Frampton MB. 2016. Tools and techniques for computational reproducibility.  
864 *Gigascience* **5**: 30.
- 865 Prendergast JGD, Tong P, Hay DC, Farrington SM, Semple CAM. 2012. A genome-wide screen  
866 in human embryonic stem cells reveals novel sites of allele-specific histone modification  
867 associated with known disease loci. *Epigenetics Chromatin* **5**: 6.
- 868 Rao S, Hoskins I, Tonn T, Garcia PD, Ozadam H, Sarinay Cenik E, Cenik C. 2021. Genes with

- 869 5' terminal oligopyrimidine tracts preferentially escape global suppression of translation by  
870 the SARS-CoV-2 Nsp1 protein. *RNA* **27**: 1025–1045.
- 871 Robles-Espinoza CD, Mohammadi P, Bonilla X, Gutierrez-Arcelus M. 2021. Allele-specific  
872 expression: applications in cancer and technical considerations. *Curr Opin Genet Dev* **66**:  
873 10–19.
- 874 Rozowsky J, Abyzov A, Wang J, Alves P, Raha D, Harmanci A, Leng J, Bjornson R, Kong Y,  
875 Kitabayashi N, et al. 2011. AlleleSeq: analysis of allele-specific expression and binding in a  
876 network framework. *Mol Syst Biol* **7**: 522.
- 877 Serrat R, Mirra S, Figueiro-Silva J, Navas-Pérez E, Quevedo M, López-Doménech G, Podlesniy  
878 P, Ulloa F, Garcia-Fernández J, Trullas R, et al. 2014. The Armc10/SVH gene: genome  
879 context, regulation of mitochondrial dynamics and protection against A $\beta$ -induced  
880 mitochondrial fragmentation. *Cell Death Dis* **5**: e1163.
- 881 Singh P, Cho J, Tsai SY, Rivas GE, Larson GP, Szabó PE. 2010. Coordinated allele-specific  
882 histone acetylation at the differentially methylated regions of imprinted genes. *Nucleic Acids*  
883 *Res* **38**: 7974–7990.
- 884 Slobodin B, Han R, Calderone V, Vrieling JAFO, Loayza-Puch F, Elkon R, Agami R. 2017.  
885 Transcription Impacts the Efficiency of mRNA Translation via Co-transcriptional N6-  
886 adenosine Methylation. *Cell* **169**: 326–337.e12.
- 887 Smith T, Heger A, Sudbery I. 2017. UMI-tools: modeling sequencing errors in Unique Molecular  
888 Identifiers to improve quantification accuracy. *Genome Res* **27**: 491–499.
- 889 Song H, Song J, Cheng M, Zheng M, Wang T, Tian S, Flavell RA, Zhu S, Li H-B, Ding C, et al.  
890 2021. METTL3-mediated m<sup>6</sup>A RNA methylation promotes the anti-tumour immunity of  
891 natural killer cells. *Nat Commun* **12**: 5522.
- 892 Tilgner H, Jahanbani F, Blauwkamp T, Moshrefi A, Jaeger E, Chen F, Harel I, Bustamante CD,  
893 Rasmussen M, Snyder MP. 2015. Comprehensive transcriptome analysis using synthetic  
894 long-read sequencing reveals molecular co-association of distant splicing events. *Nat*  
895 *Biotechnol* **33**: 736–742.
- 896 Tilgner H, Jahanbani F, Gupta I, Collier P, Wei E, Rasmussen M, Snyder M. 2018. Microfluidic  
897 isoform sequencing shows widespread splicing coordination in the human transcriptome.  
898 *Genome Res* **28**: 231–242.
- 899 Tsang S, Sun Z, Luke B, Stewart C, Lum N, Gregory M, Wu X, Subleski M, Jenkins NA,  
900 Copeland NG, et al. 2005. A comprehensive SNP-based genetic analysis of inbred mouse  
901 strains. *Mamm Genome* **16**: 476–480.
- 902 Vantourout P, Laing A, Woodward MJ, Zlatareva I, Apolonia L, Jones AW, Snijders AP, Malim  
903 MH, Hayday AC. 2018. Heteromeric interactions regulate butyrophilin (BTN) and BTN-like  
904 molecules governing  $\gamma\delta$  T cell biology. *Proc Natl Acad Sci U S A* **115**: 1039–1044.
- 905 Viscardi MJ, Arribere JA. 2022. Poly(a) selection introduces bias and undue noise in direct  
906 RNA-sequencing. *BMC Genomics* **23**: 530.
- 907 Wang H, Coligan JE, Morse HC 3rd. 2016. Emerging Functions of Natural IgM and Its Fc

- 908 Receptor FCMR in Immune Homeostasis. *Front Immunol* **7**: 99.
- 909 Wang S, Lv W, Li T, Zhang S, Wang H, Li X, Wang L, Ma D, Zang Y, Shen J, et al. 2022.  
910 Dynamic regulation and functions of mRNA m6A modification. *Cancer Cell Int* **22**: 48.
- 911 Wang X, Lu Z, Gomez A, Hon GC, Yue Y, Han D, Fu Y, Parisien M, Dai Q, Jia G, et al. 2014.  
912 N6-methyladenosine-dependent regulation of messenger RNA stability. *Nature* **505**: 117–  
913 120.
- 914 Wick RR, Judd LM, Holt KE. 2019. Performance of neural network basecalling tools for Oxford  
915 Nanopore sequencing. *Genome Biol* **20**: 129.
- 916 Wilson DJ. 2019. The harmonic mean  $p$ -value for combining dependent tests. *Proc Natl Acad*  
917 *Sci U S A* **116**: 1195–1200.
- 918 Workman RE, Tang AD, Tang PS, Jain M, Timp W. 2018. Nanopore native RNA sequencing of  
919 a human poly(A) transcriptome.  
920 [https://www.researchgate.net/publication/328855598\\_Nanopore\\_native\\_RNA\\_sequencing\\_of\\_a\\_human\\_polyA\\_transcriptome](https://www.researchgate.net/publication/328855598_Nanopore_native_RNA_sequencing_of_a_human_polyA_transcriptome) (Accessed December 13, 2023).  
921
- 922 Wu J, Hu W, Li S. 2023. Long-read transcriptome sequencing reveals allele-specific variants at  
923 high resolution. *Trends Genet* **39**: 31–33.
- 924 Yang X, Triboulet R, Liu Q, Sendinc E, Gregory RI. 2022. Exon junction complex shapes the  
925 m6A epitranscriptome. *Nat Commun* **13**: 7904.
- 926 Yoav Benjamini YH. 1995. Controlling the False Discovery Rate: A Practical and Powerful  
927 Approach to Multiple Testing. *J R Stat Soc* **57**. <https://www.jstor.org/stable/2346101>.
- 928 Zhang Z, Chen T, Chen H-X, Xie Y-Y, Chen L-Q, Zhao Y-L, Liu B-D, Jin L, Zhang W, Liu C, et  
929 al. 2021. Systematic calibration of epitranscriptomic maps using a synthetic modification-  
930 free RNA library. *Nat Methods* **18**: 1213–1222.
- 931 Zheng D, Wang J, Persyn L, Liu Y, Montoya FU, Cenik C, Agarwal V. 2024. Predicting the  
932 translation efficiency of messenger RNA in mammalian cells. *bioRxiv*.  
933 <http://dx.doi.org/10.1101/2024.08.11.607362>.
- 934 Zitovsky JP, Love MI. 2019. Fast effect size shrinkage software for beta-binomial models of  
935 allelic imbalance. *F1000Res* **8**: 2024.
- 936

937 **FIGURE LEGENDS**

938

939 **Figure. 1 | Allelic read assignment and m6A modification analysis using ONT DRS in hybrid**  
940 **mESCs**

941 A) M6A modification ratio and locations detected from m6Anet using all reads (top, green, WT;  
942 bottom, red, *Mettl3* knockout). The relative m6A locations within the transcript body were  
943 determined. It presents modification ratios after high probability selection ( $> 0.85$ ). The color  
944 darkness represents the counts of the ratio on the position. B) Comparison of the frequencies of  
945 instances of DRACH motif sequences (green, WT; red, *Mettl3* knockout). C) Schematic overview  
946 of the strategy used for allelic long-read assignment for allele-specific m6A modification analysis.  
947 Total RNA from hybrid mESC (C57BL/6J  $\times$  CAST/EiJ) underwent DRS. To avoid reference bias,  
948 we used an N-masked transcriptome for alignment. Reads were then allocated to each allele.  
949 This process classified reads into Allele A (B6), Allele B (CAST), and undefined categories,  
950 enabling m6A detection within each group individually.

951

952 **Figure. 2 | Comparative analysis of allelic modifications in wild-type and *Mettl3* knockout**  
953 **mESCs**

954 A) Allelic impartiality while allelic read assignment and m6A detection. The left pane outlines the  
955 schematic of the data procedural steps for allele-specific m6A modifications analysis. The right  
956 panels display the counts for allelic reads, candidate m6A sites, and high probability m6A sites  
957 selected through our criteria (red circles, B6; blue plusses, CAST; and gray triangles, undefined  
958 group). The left top two plots show the counts from mESC wild-type (WT) replicates and the  
959 bottom plot exhibits the numbers from mESC *Mettl3* knockout. B) Spearman's correlation of  
960 modification ratio between alleles from wild-type and *Mettl3* knockout cells (rep1: mESC WT  
961 replicate 1; rep2: mESC WT replicate 2; *Mettl3*: *Mettl3* knockout). C-D) Distribution of sites with  
962 high probability of m6A modification (prob  $> 0.85$ ) is displayed in a metagene plot by calculating

963 the relative positions of these sites within gene regions. The color scale represents the number  
964 of m6A sites with the given modification ratio inferred from reads assigned to either of the two  
965 alleles in mESC wild-type (C) or *Mettl3* knockout (D) cells (red, B6 allele; blue, CAST allele).

966

### 967 **Figure. 3 | Identification and classification of ASM sites**

968 A) Schematic of statistical procedure for ASM detection (Methods). Reads overlapping the site  
969 under consideration were resampled, and the modification ratio was estimated in each bootstrap  
970 sample. A statistically significant ASM site was defined as adjusted harmonic p-value ( $FDR < 0.1$ ;  
971 Methods). B) An ASM site within *Trim25*, exhibits distinct modification ratio samples. Conversely,  
972 a non-ASM site within *Trim59* displays substantial overlap in modification ratios between  
973 bootstrap sampling distributions. C) Modification ratios of each allele across mESC wild-type  
974 replicates. Y-axis displays the name of the gene and m6A position in the transcript. D-E) ASM  
975 sites were classified into two groups. Group 1 is defined by genetic variants within the DRACH  
976 motif, and Group 2 is characterized by variants adjacent to or distal from the DRACH motif (D).  
977 The modification differences of the defined ASM were represented by color according to their  
978 classification (Group 1 in magenta, Group 2 in blue, and non-ASM in gray). Each axis is the  
979 modification ratio, where negative values denote CAST allele bias and positive values indicate  
980 B6 allele bias in m6A modification (E).

981

### 982 **Figure. 4 | Characterization of ASM sites and orthogonal detection with MeRIP-seq**

983 A) SNP distribution in Group 1 ASM. B) Motif frequencies and modification ratios of motif  
984 sequences. The top bar plot illustrates motif sequence frequencies in all m6A instances, while the  
985 bottom heatmap indicates modification ratios. The first row presents modification ratio of all  
986 instances and the following six rows represents modification ratio on each motif sequence  
987 differentiated by SNPs from two alleles of Group 1 ASM sites. C) Information content of the  
988 extended DRACH motif in 17 Group 2 ASM sites shown in DNA sequence. The D-1 site has three

989 SNPs, while the H+1 and H-2 sites each have one SNP. D) Extended motif sequences where the  
 990 D-1 site possesses SNPs. The gray box represents the DRACH motif, in which all three genes  
 991 share the same sequence (UGACU) followed by U on the D-2 site. E) Motif prevalence in Group  
 992 2 ASM. The UGACU motifs are predominantly observed, contrasting with the common m6A motifs,  
 993 which are typically represented by GGACU. F-G) Orthogonal detection of ASM through MeRIP-  
 994 seq and long-read sequencing. On the top panel, points illustrate the allele-bias m6A ratio  
 995 (proportion of reads from CAST allele) derived from three replicates of MeRIP-seq analysis. The  
 996 Integrated Genome Viewer browser displays MeRIP-seq reads on SNPs adjacent to m6A sites,  
 997 which correspond to the MeRIP-seq allele-bias ratio. The points in the bottom panel indicate the  
 998 modification ratio of each allele from long-read sequencing, with gray color pairs representing  
 999 data from two replicates. Two examples from *Apt5o*, Group 1 ASM (F) and *Gcsh*, Group 2 ASM  
 1000 (G) are shown.

1001

### 1002 **Figure. 5 | Reproducibility of ASM profiling procedure in human cells**

1003 A) Number of detected candidate m6A modification sites among five replicates (blue, Allele A;  
 1004 orange, Allele B; gray, undefined read classification). B) Modification ratios from each allele,  
 1005 including three ASM sites (blue) and non-ASM sites (gray) in UCSC (left) and UN (right) datasets,  
 1006 the highest depth datasets among five replicates. The X-axis represents the modification ratio of  
 1007 Allele A reads, while the Y-axis represents the modification ratio of Allele B reads. C) Resampled  
 1008 modification ratios from bootstrapping. Each color represents an allele (blue for Allele A, orange  
 1009 for Allele B), and the gray gradient indicates each replicate.

1010

### 1011 **Figure 6 | Effects of ASM on allele specific RNA expression and ribosome occupancy**

1012 A) Allele bias ratio of genes containing ASM sites (sky blue for B6 biased; pink for CAST biased).  
 1013 Different shapes represent the replicates (circle for replicate 1, triangle for replicate 2) The Y-axis  
 1014 displays the allele bias ratio obtained from long-read (left), short-read (middle) sequencing, and

1015 ribosome profiling (right). The X-axis shows the difference in m6A modification ratios between the  
1016 two alleles (CAST - B6). The red dashed horizontal bar indicates allele-bias ratio 0.5, an allele-  
1017 bias cutoff point. The gray bar represents the mean allele bias ratio for genes with B6 or CAST  
1018 biased ASM sites. B) Model for regulation of ASM and allele-specific expression. The two-sided  
1019 arrow in the model reflects the possibility of bidirectional influence, rather than suggesting  
1020 unidirectional causality. Differential transcription driven by allele-specific epigenetic contexts may  
1021 regulate ASM, indicating that both phenomena could share a common underlying mechanism,  
1022 without one necessarily being the direct cause of the other.

# Figure 1

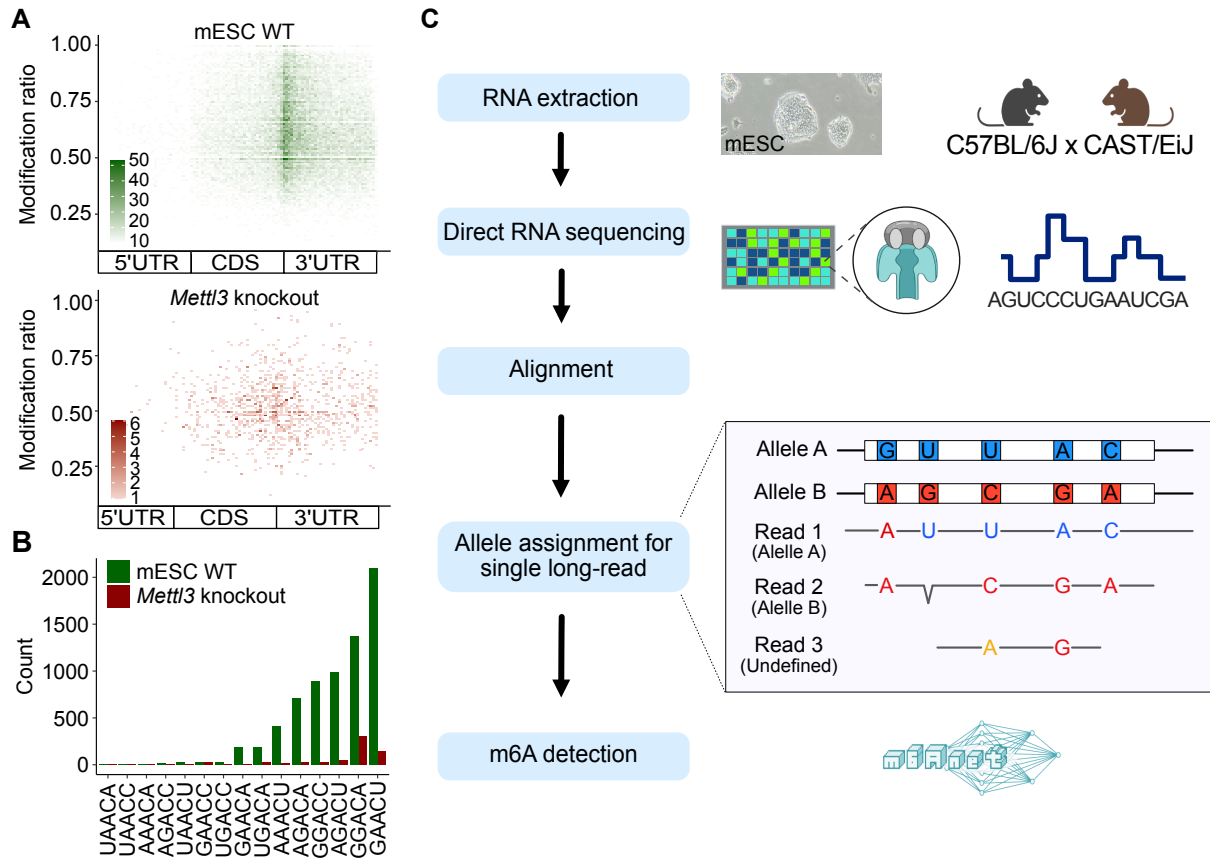




# Figure 3

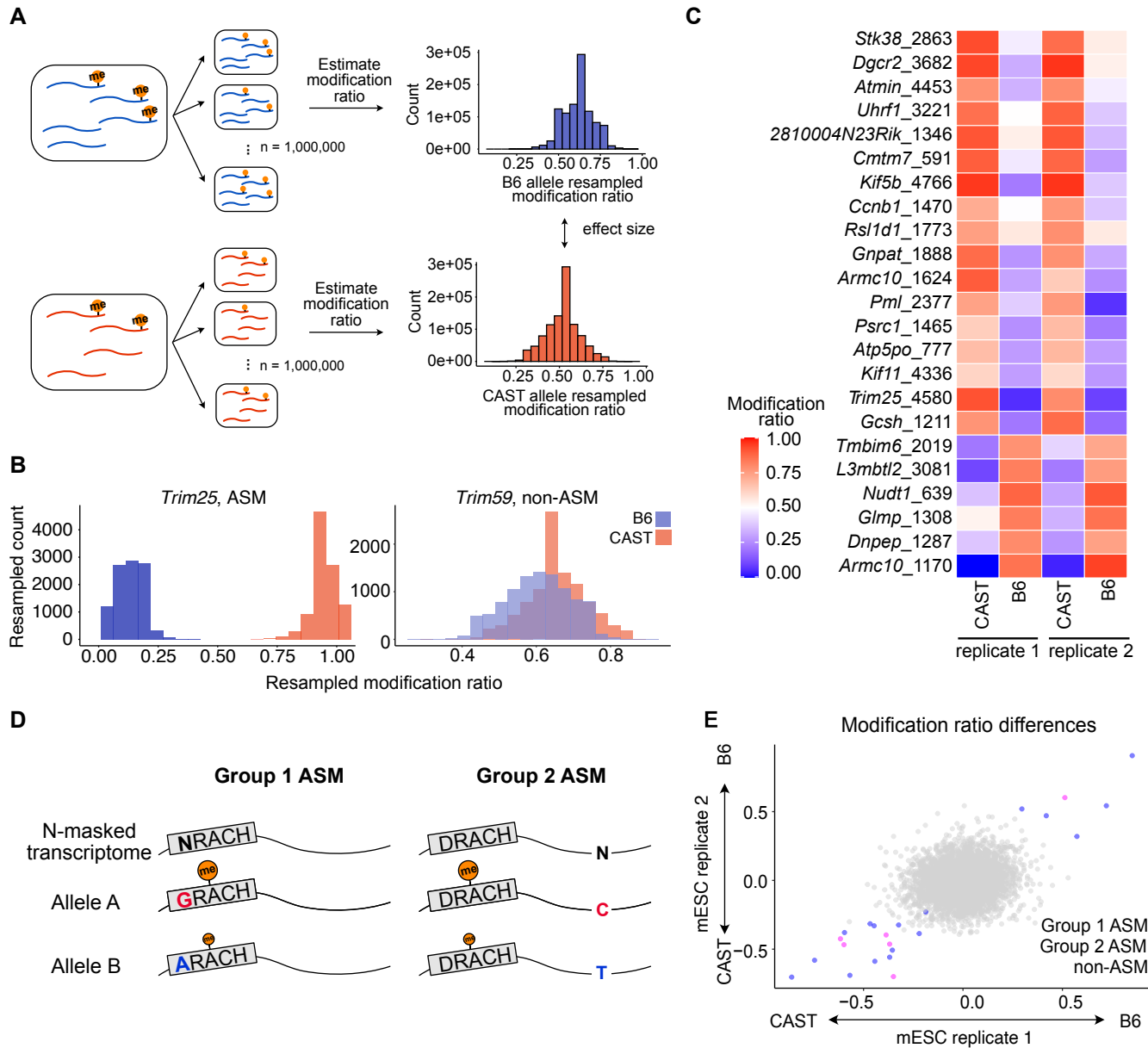


# Figure 4

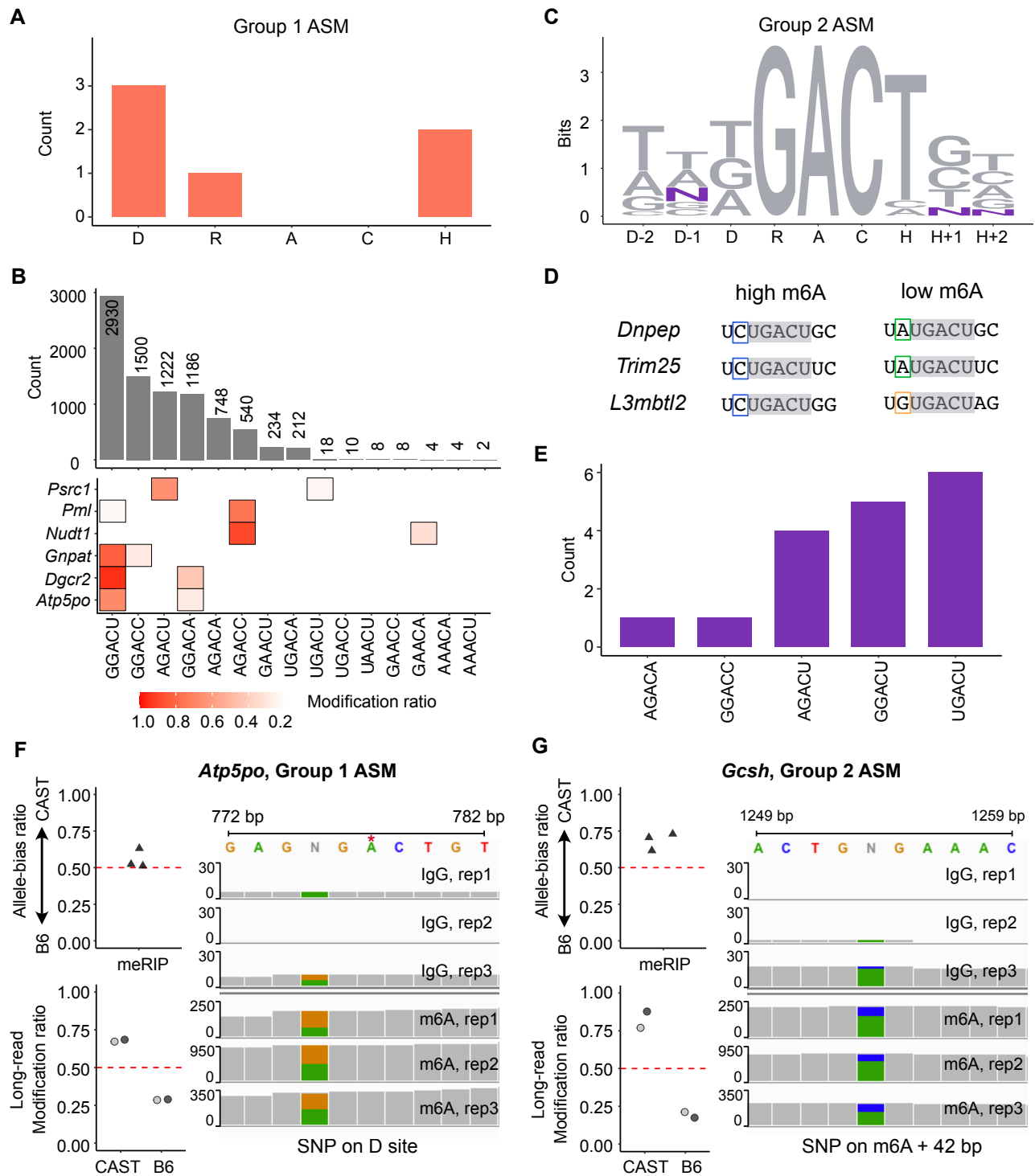


# Figure 5

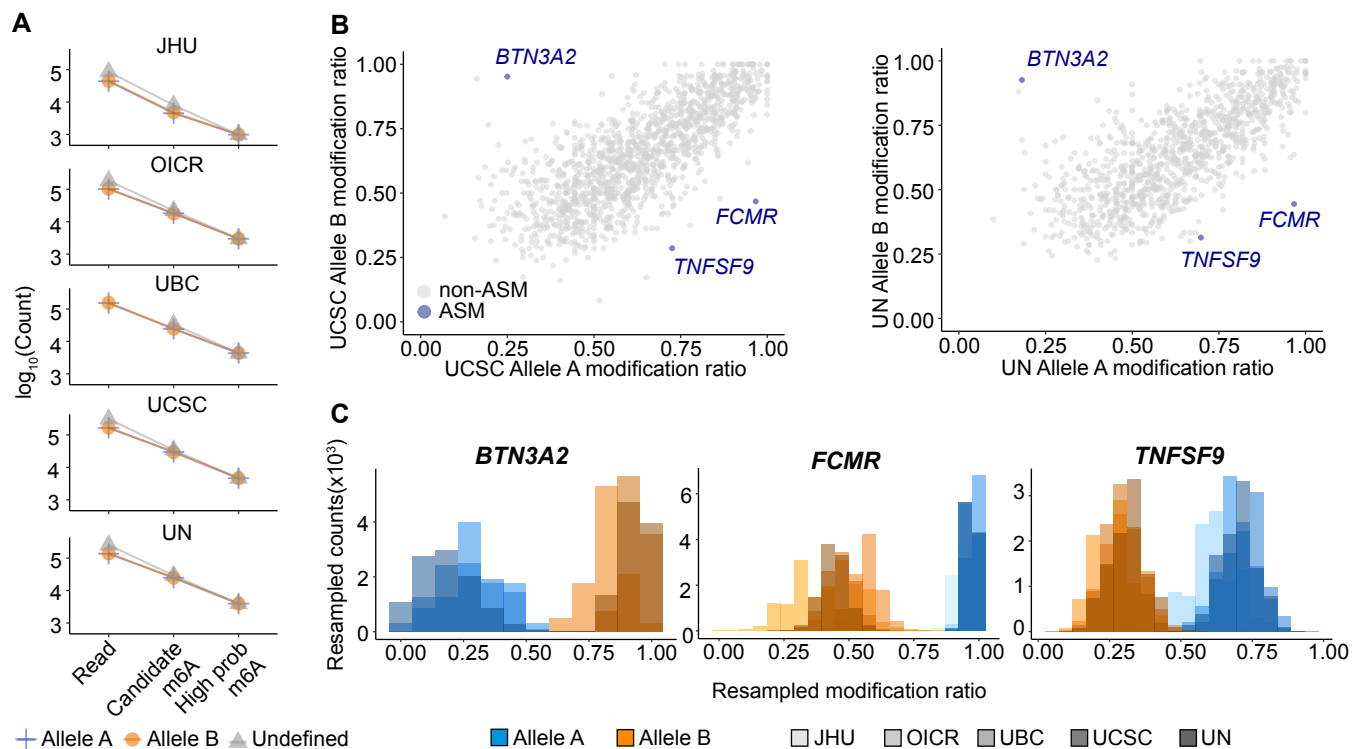


# Figure 6

